# Adaptive Active Control of Sound Fields in Elastic Cylinders via Vibrational Inputs

D. S. Mandic* and J. D. Jones†
*Purdue University, West Lafayette, Indiana 47907*

**A simplified cylindrical model of an aircraft fuselage is used to evaluate an active noise control system using vibrational force inputs as secondary control sources. Horn drivers are used to simulate propeller-induced cabin noise while a mini-shaker attached pointwise to the shell wall is used as the control source. The cylindrical shell is unstiffened, undamped, and contains no interior acoustic damping. A control system based on the filtered-$x$ version of the least mean squares algorithm is configured to reduce the interior noise level of the cylinder, using one control source and one error sensor (interior microphone). Control at three discrete frequencies corresponding to dominant acoustic cavity modes of the test shell is demonstrated, as well as control of two modes simultaneously. Additionally, one test was conducted using a second mini-shaker as the primary source in place of the acoustic drivers, to simulate a condition of local vibrational energy flow into the fuselage. Results for all cases are fully documented, including the spatial extent of control in the source plane. Global reductions as high as 28 dB of the interior acoustic field are demonstrated, with minimal increases in shell vibration.**

## Introduction

ATTENUATION of blade passage noise in turboprop aircraft is a challenging task. Strong, low-frequency harmonics characteristic of propeller-induced cabin noise are difficult to attenuate using traditional passive measures without incurring an excessive weight penalty. With the advent of advanced turboprop (ATP) engines, control of low-frequency cabin noise becomes a critical issue because ATP propellers can create noise levels in excess of 150 dB at the fuselage sidewall.[1] Alternative methods of controlling the sound transmission into the aircraft interiors are currently being studied in order to make these aircraft suitable for commercial use. Active noise control (ANC) has shown promise as an alternative lightweight control strategy for reducing low-frequency cabin noise in conventional as well as future turboprop aircraft.

The application of ANC to the aircraft environment was first demonstrated in 1984 by Zalas and Tichy[2] with limited success. Significant reductions of the blade passage noise were achieved, but the spatial extent of reduction was highly localized (local control). Thus, subsequent investigations[3-8] returned to simple laboratory models in order to better understand what is required to spatially recreate the primary sound field using secondary control actuators, and hence provide reduction over a larger interior volume (global control).

In general, two ANC methods have been investigated. The first more conventional method[3-5] involves the use of an array of interior acoustic control sources to recreate the enclosed sound field. The second method[6-8] makes use of pointwise attached vibrational control actuators to directly control the vibrational response of the enclosure, and consequently, reduce sound transmission into the enclosure. Recent ground and in-flight tests of these methods in aircraft cabins have shown promise.[9,10]

Although the results of previous studies using vibrational control forces[6-8] are encouraging, the control systems used in each of the studies was limited to single sinusoidal inputs. The focus of this new study is to expand on previous work by designing an adaptive active vibration control system to reduce pure tone as well as multiharmonic noise in a similar aircraft model. A different control strategy employing adaptive digital filtering was chosen, and a single input/single output system with one error sensor was developed. This paper documents the problems associated with the new control strategy as well as initial experimental results that were achieved.

## Experimental Configuration

A diagram of the simplified aircraft model used for this study is shown in Fig. 1. The test article consists of a steel cylinder, 1.68 m (66 in.) long by 0.838 m (33 in.) in diameter by 1.588 mm (1/16 in.) thick, sealed with wooden endcaps.

For this initial study, the cylinder was left undamped, both structurally and acoustically. Although this is not characteristic of an actual fuselage, it enabled better prediction and subsequent analysis of the results because the modal nature of the system was known from separate modal analyses conducted on the cylindrical shell and the interior acoustic space. A pair of horn drivers was used to provide a single, localized, monopole-type acoustic source located at the axial center on one side of the cylinder (designated $\theta = 0$ deg). Control input was

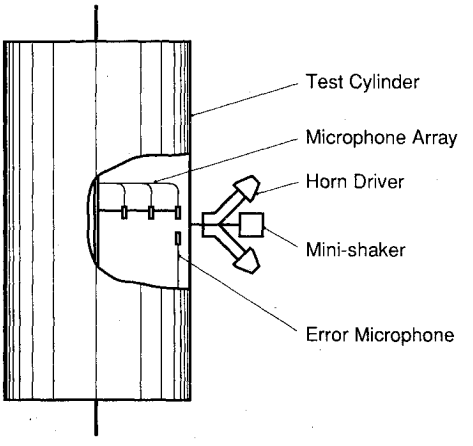


**Fig. 1 Schematic diagram of the fuselage model.**

Presented as Paper 89-1075 at the AIAA 12th Aeroacoustics Conference, San Antonio, TX, April 10-12, 1989; received Dec. 20, 1989; revision received Sept. 20, 1990; accepted for publication Sept. 26, 1990. 

*Graduate Research Assistant, Ray W. Herrick Laboratories, School of Mechanical Engineering; currently with the General Motors Noise and Vibration Laboratory, Milford Proving Ground, Milford, MI 48380.

†Associate Professor, Ray W. Herrick Laboratories, School of Mechanical Engineering. Member AIAA.

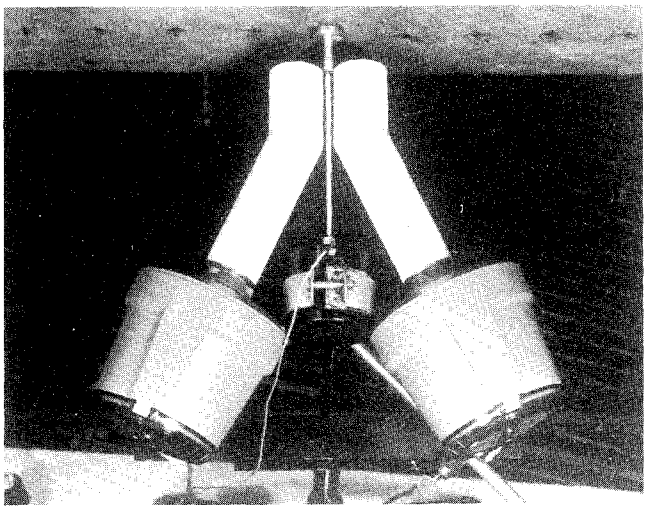

Fig. 2 Horn drivers and control shaker.

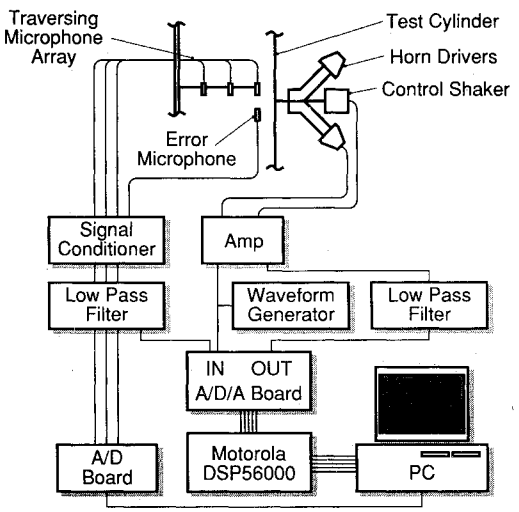


Fig. 3 Data acquisition system.

provided by a mini-shaker located between the horn drivers and attached pointwise to the cylinder using a swivel stinger. Figure 2 shows the horn driver/shaker arrangement (photo).

Pressure response inside the cylinder is monitored using an array of three 12 mm (1/2 in.) condenser microphones mounted on a traverse mechanism at nondimensional radial locations $r/a = 0.1, 0.5$, and 0.9, where $a$ is the inner radius of the shell. The traverse can sweep the cavity both axially and circumferentially, although only circumferential data is presented here. An additional interior microphone is separately mounted in the cavity directly opposite the minishaker (at $\theta =$ 0 deg) and is used as an error sensor for the control program.

An arbitrary waveform generator was used to provide sinusoidal signals to the horn drivers. This signal was also used as a detector signal for the control system to avoid positive acoustic feedback. Acoustic feedback can be avoided in practice by using an exterior microphone or a filtered engine tachometer signal, among other methods.

Figure 3 contains a diagram of the data acquisition and processing system. The control algorithm runs on a Motorola DSP56000 Application Development System (ADS) digital signal processing board. The digital signal processing (DSP) board is connected to its own dedicated analog interface (analog-to-digital and digital-to-analog converter board) and has an interface card mounted in a microcomputer for transmission of program code and other instructions. As shown in Fig. 3, the DSP board reads a detector signal from the reference oscillator and an error signal from an interior microphone. Based on these signals, the processor computes a control signal using the methods described in the following section.

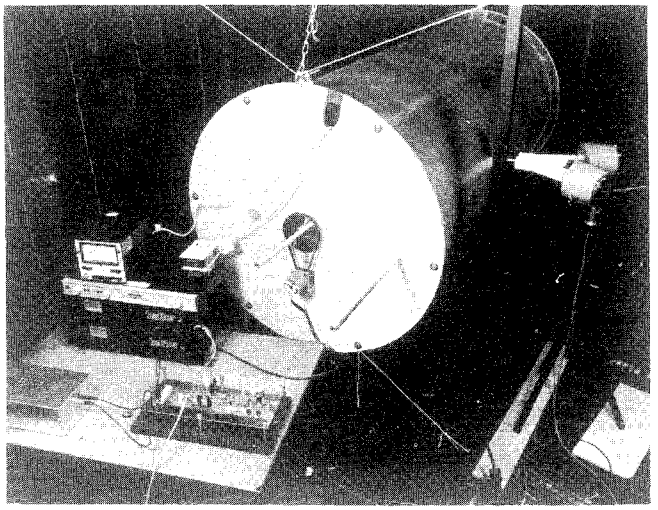

Fig. 4 Test apparatus.

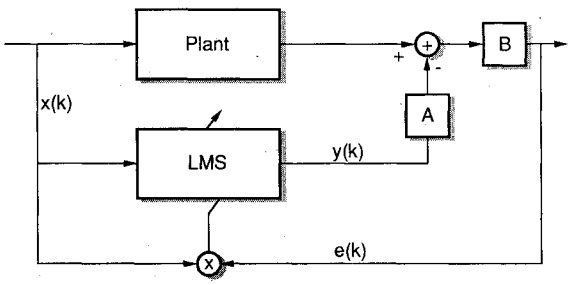


Fig. 5 Block diagram of a basic LMS control system.

The three microphones mounted on the traverse mechanism are used to evaluate the sound field interior to the cylinder before and after the control system is applied. The microphone signals are read using another analog-to-digital conversion board mounted directly in the microcomputer. The results are then processed and stored in data files on disk. The traverse mechanism is automatically rotated using a stepper motor controlled by the data acquisition program (shown in Fig. 4). Note that all signals are processed using low pass filters to prevent aliasing in input data and provide smoothing for the control signal.

## Control Algorithm

The control algorithm used in this study is based on the least mean squares (LMS) algorithm.[11] The basic LMS algorithm reads a disturbance (detector) signal $x_k$, and uses a finite impulse response (FIR) filter to compute the control output $y_k$:

$$y_k = \sum_{i=0}^{N} h_i x_{k-i} \tag{1}$$

The $h_i$ in Eq. (1) are the coefficients of the FIR filter, $N$ is the length of the filter, and $k$ represents digital time. The control output is sent to a control source, where it will physically add with some original noise signal, ideally cancelling it. An error signal $e_k$ is read with an interior microphone and is used to modify the filter coefficients after each iteration, according to

$$h_i(k+1) = h_i(k) + 2\mu e_k x_{k-i} \tag{2}$$

The constant $\mu$ is the adaption gain, which controls the speed of convergence of the coefficients. This entire process is shown in block diagram form in Fig. 5.

Note that there are four transfer functions in Fig. 5: a plant, or physical acoustic system to be controlled; an LMS control filter, which is modeling the plant; and the blocks labeled A and B, which represent the error path transfer functions of all components between the output of the control signal $y_k$ and the input of the error signal $e_k$ to the controller. For a typical ANC system, the error path would include the transfer functions of the control source (e.g., loudspeaker or shaker), the physical path between the control source and the error microphone (e.g., the response of the cylindrical shell and the transport time delay of the acoustic path), and the error microphone itself, as well as the amplifiers, signal conditioners, low pass filters, and other items along the way. The combination of these transfer functions are commonly referred to as the error path.

The components of the error path are not modeled by the LMS algorithm outlined here. Because of this, they may potentially cause the system to be unstable. If the dynamics of the error path are negligible, then the LMS algorithm will converge, if the adaption gain is sufficiently small. However, the error path for most ANC systems contains a large pure time delay. In addition, the error path for this study contains a very resonant system (the cylinder and its internal acoustic space). The effects of these components must be modeled in the control program or convergence is not guaranteed.

An expanded version of the LMS algorithm, known as the filtered-$x$ LMS algorithm,[11] uses a model of the error path to filter the input signal $x_k$ before it is used in the update equation (see Fig. 6). This process can be used to correct the input signal $x_k$ for the dynamics of the error path as well as for any time delay associated with it. To find a model of the error path, the control program computes pseudorandom noise, sends this to the control source, reads the error signal, and uses the LMS algorithm to adapt another FIR filter being used to model the error path (see Fig. 7). Since the disturbance being used for input is broad in frequency content, the coefficients will converge to the impulse response of the error path (including any time delay in the path), given that a sufficient filter length is used. After a sufficient amount of time has passed, this modeling process is halted and the coefficients of the error path model are used directly in the control system as shown in Fig. 6.

The control algorithm was implemented on the Motorola DSP56000 based digital signal processing system. For all cases presented, the algorithm operated at a sampling speed of 5 kHz with filter lengths of 120 coefficients for the control filter and 430 coefficients for the error path model. While 430 coefficients may seem quite large for modeling the error path, in fact, the filter was still too small to fully represent the impulse response of the vibro-acoustic system defined by the cylinder. Since no damping material was used, the actual impulse response decayed very slowly with time, with significant amplitude reduction occurring only after about 600 ms. The filter modeling the error path, on the other hand, could only model about 100 ms of the impulse response (as configured). This model was sufficient for most of the cases tested; the algorithm converged quite readily and provided excellent control. However, at certain frequencies, the algorithm diverged, due to the poor error path model. For these cases, convergence could be forced by simply reversing the sign in the update equation [Eq. (2)]. This was sufficient for evaluating single frequency inputs, but this could not be performed for broadband signals or multitonal inputs requiring different update equations.

Because of timing constraints, the error path filter could not be made any larger. It appears that, to model this type of system, an infinite impulse response filter (IIR) would be more suitable than the FIR filter outlined here. An IIR filter provides a pole/zero model of the system rather than the all-zero model provided by an FIR filter. However, IIR filters are inherently unstable, and a number of new problems arose when this type of modeling was attempted. For this reason, the FIR model was used for this study.

Since most practical environments contain higher levels of damping, some damping material was subsequently added to the cylinder and its interior acoustic space. A better model of the error path was found, with a corresponding increase in the robustness of the algorithm. However, the modal properties of the system changed drastically, and the results of control at different frequencies were not as clear.

## Experimental Procedure

All tests were performed in the anechoic chamber at Herrick Laboratories. The harmonic primary source was adjusted to provide suitable interior sound pressure levels, typically 100–110 dB (re 20 $\mu$Pa). In order to characterize the error path, the controller first drives the control shaker with pseudorandom noise, reads the error microphone signal, and based on the input/output records, identifies the impulse response of the error path, as described earlier. This process continues for approximately 20 s before it is automatically terminated. The controller then begins executing the ANC portion of the program, continually adapting in order to minimize the pressure variation at the error sensor. Once the controlled system reaches steady state, the adaption process is terminated and the data acquisition program running on the microcomputer is initiated. This program reads the traverse microphone signals, performs fast Fourier transforms and averages the data, and then stores the results (magnitude and phase) to disk files. The program uses a stepper motor to automatically rotate the microphone array to the next position, where the process repeats. Data were acquired at 24 equally spaced angular positions for each case.

Once data have been collected at all 24 locations, they are further reduced into a series of orthogonal modes by a spatial Fourier decomposition process.[12] Basically, the process assumes the complex pressure amplitudes $w(\theta,t)$ can be represented as a Fourier series of sine and cosine functions:

$$w(\theta,t) = \sum_{n=0}^{12} [a_n \cos(n\theta) + b_n \sin(n\theta)] e^{j\omega t} \qquad (3)$$

The decomposition process identifies the relative modal amplitudes of the interior sound field, with the symmetric $a_n$ modes having a $\cos(n\theta)$ distribution and the asymmetric $b_n$ modes having a $\sin(n\theta)$ distribution. Note that only the $n = 0$ through 12 modes can be identified since $w(\theta,t)$ is only known at 24 discrete points (for each radial microphone location). Decom-

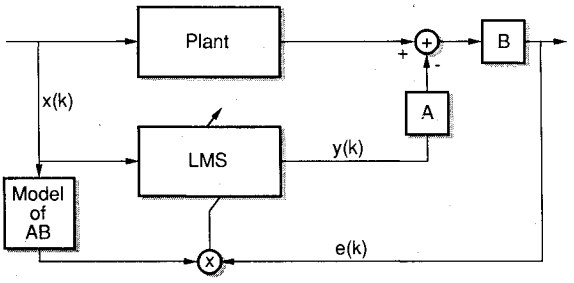


Fig. 6 Block diagram of the filtered-$x$ LMS algorithm.

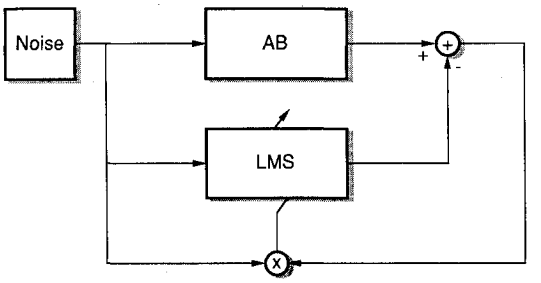


Fig. 7 Block diagram of the error path modeling process.

position is performed separately on data from each of the interior microphones. Only results for the outer microphone ($r/a$ = 0.9) are presented, as they are representative of the results observed at all three microphone locations.

Once this entire process has concluded for the composite (controlled) field, it is repeated first with the primary source switched off and then with the secondary source deactivated and the primary source on. In this manner, data for the primary, secondary, and composite sound field are gathered for each test case.

For one of the tests, the associated structural response of the test cylinder was also evaluated. Acceleration data were acquired at 40 equally spaced angular positions for each case (primary, secondary, and composite). As with the pressure data, the measured shell response was decomposed into its relative modal amplitudes ($a_n$ and $b_n$), using the Fourier decomposition method discussed previously.

## Results and Discussion

Five separate tests are presented here. For the first three tests, the system was evaluated while the acoustic source was driven at a single tone. The frequencies chosen for these tests (340, 413, and 450 Hz) correspond to three dominant acoustic cavity modes of this system. Test four was conducted with an input of two pure tones (413 and 450 Hz) to demonstrate control of two modes simultaneously. Finally, for test five, a second mini-shaker located at $\theta$ = 180 deg was used as a primary source in place of the horn drivers.

**Test 1: 340 Hz**

The system was driven at 340 Hz for this case. The level of reduction in sound pressure level (SPL) was 56.8 dB at the error sensor, while the spatially averaged reduction was determined to be 9.8 dB (in the source plane). It was known a priori from an experimental modal analysis of the acoustic cavity that the $n$ = 1 circumferential mode dominates the interior acoustic space at this frequency.

Contour plots of the primary, secondary, and composite sound fields are shown in Fig. 8 and, as expected, the $n$ = 1 acoustic mode appears to dominate the interior sound field. Not expected, however, was the manner in which the $n$ = 1 mode aligned itself. Note that the $n$ = 1 mode is composed of two orthogonal modes corresponding to $a_1 \cos(\theta)$ and $b_1 \sin(\theta)$. Since the primary and secondary sources are both located at $\theta$ = 0 deg, as shown in the figure, it was expected that the antinodes of their respective interior responses would line up at $\theta$ = 0 deg (i.e., the $a_1$ mode would dominate the field). Instead, the antinodes were located at approximately $\theta$ = 45 deg and 135 deg ($\theta$ measured counterclockwise). Correspondingly, a node of the interior sound field was located at $\theta$ = 45 deg, which is near a welded seam in the cylinder.

The Fourier decomposition of the pressure data (see Fig. 9) shows that, for both the primary and secondary fields, the $b_1$ mode, which has a node at $\theta$ = 0 deg, was excited more strongly than the $a_1$ mode, which has an antinode at $\theta$ = 0 deg. It should be noted that this driving frequency excites a strong resonance of this undamped system, and thus will cause

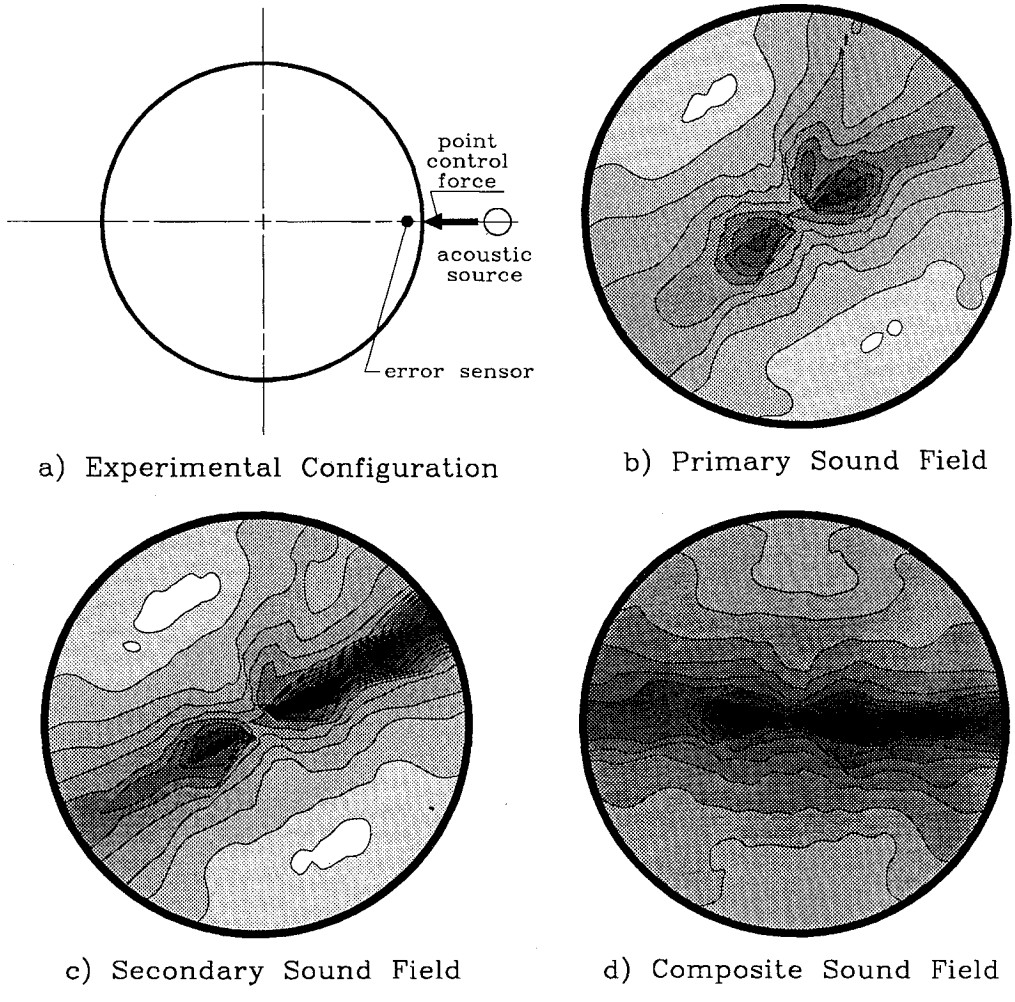


**Fig. 8 Contour maps of the source plane, driving frequency of 340 Hz.**

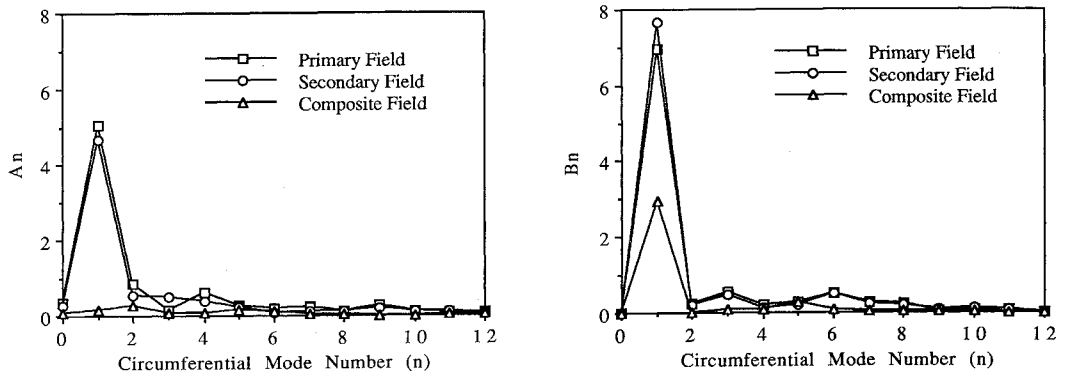


**Fig. 9 Relative modal amplitudes of pressure response in the source plane at 340 Hz: □, primary field; ○, secondary field; △, composite field.**

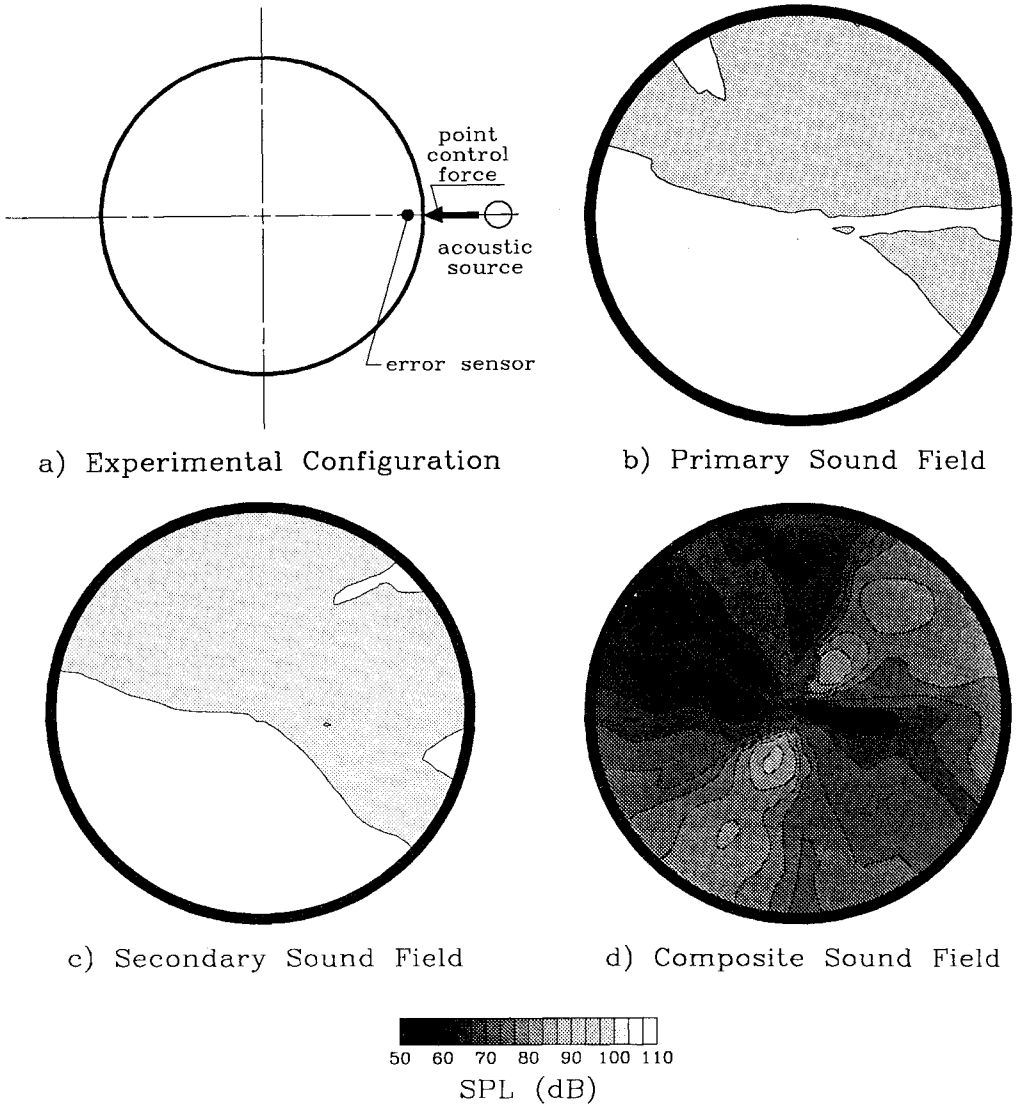


**Fig. 10 Contour maps of the source plane, driving frequency of 413 Hz.**

alignment of the responding mode shape to be affected by the inhomogeneities of the system, as well as the location of the actuator. For a perfectly homogeneous cylinder, it would be expected that antinodes of the modes excited would occur at the location of the forcing actuator. If the system is not perfectly homogeneous, then physical geometry of the system will affect the location of the antinodes for the excited modes.[7,8] The cylinder used for the current study has a welded joint at approximately $\theta = 45$ deg, as well as two interior microphone mounting structures and their corresponding microphones and cables. Other factors include the stiffening and mass loading effect of the mini-shaker attachment, misalignments in actuator mounting, and variations in the shell wall itself. These factors may all contribute to the mode shifting that has been observed. It is expected that, as damping material is added to the system, the antinodes of interior field will line up more closely with the actuators.

The composite field, on the other hand, shows results that are more predictable. The contour plot for the composite field shows that the $a_1$ mode was completely suppressed, leaving the $b_1$ mode dominating the sound field. The Fourier decomposition (Fig. 9) shows this phenomenon more clearly. These

results were expected since the error sensor was located at $\theta$ = 0 deg, an antinodal point for the $a_1$ mode and a nodal point for the $b_1$ mode. Since the control algorithm minimizes the sound field at the location of the error sensor, it will tend to minimize the magnitude of the $a_1$ mode. Conversely, the control system is "blind" to the level of excitation of the $b_1$ mode, both before and after control, since the error sensor is at a nodal point of that mode. Hence, the level of the $b_1$ mode will combine with the $b_1$ mode created by the primary source, but in general the magnitude of these two individual components will not be equal, and it is not guaranteed that they will be opposite in phase (as is the case for the $a_1$ mode). Thus, the resulting overall magnitude of the $b_1$ mode will be determined by the physical geometry of the system, and not the controller. For this case, the $b_n$ mode, due to the primary and secondary sources, does appear to be reasonably well-matched for control (both in amplitude and phase), thus resulting in a notable drop in the level of the $b_1$ modal amplitude. However, to simultaneously control both the $a_1$ and $b_1$ modes, another error sensor located near the antinode of the $b_1$ mode would be

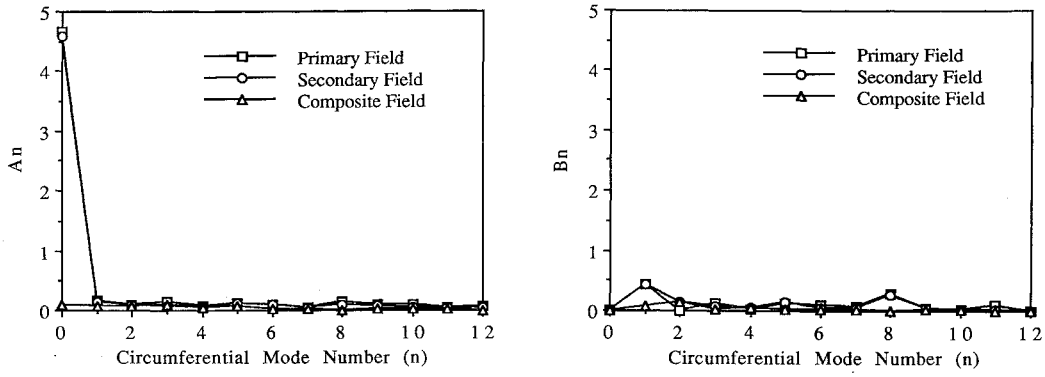


**Fig. 11 Relative modal amplitudes of pressure response in the source plane at 413 Hz: □, primary field; ○, secondary field; △, composite field.**

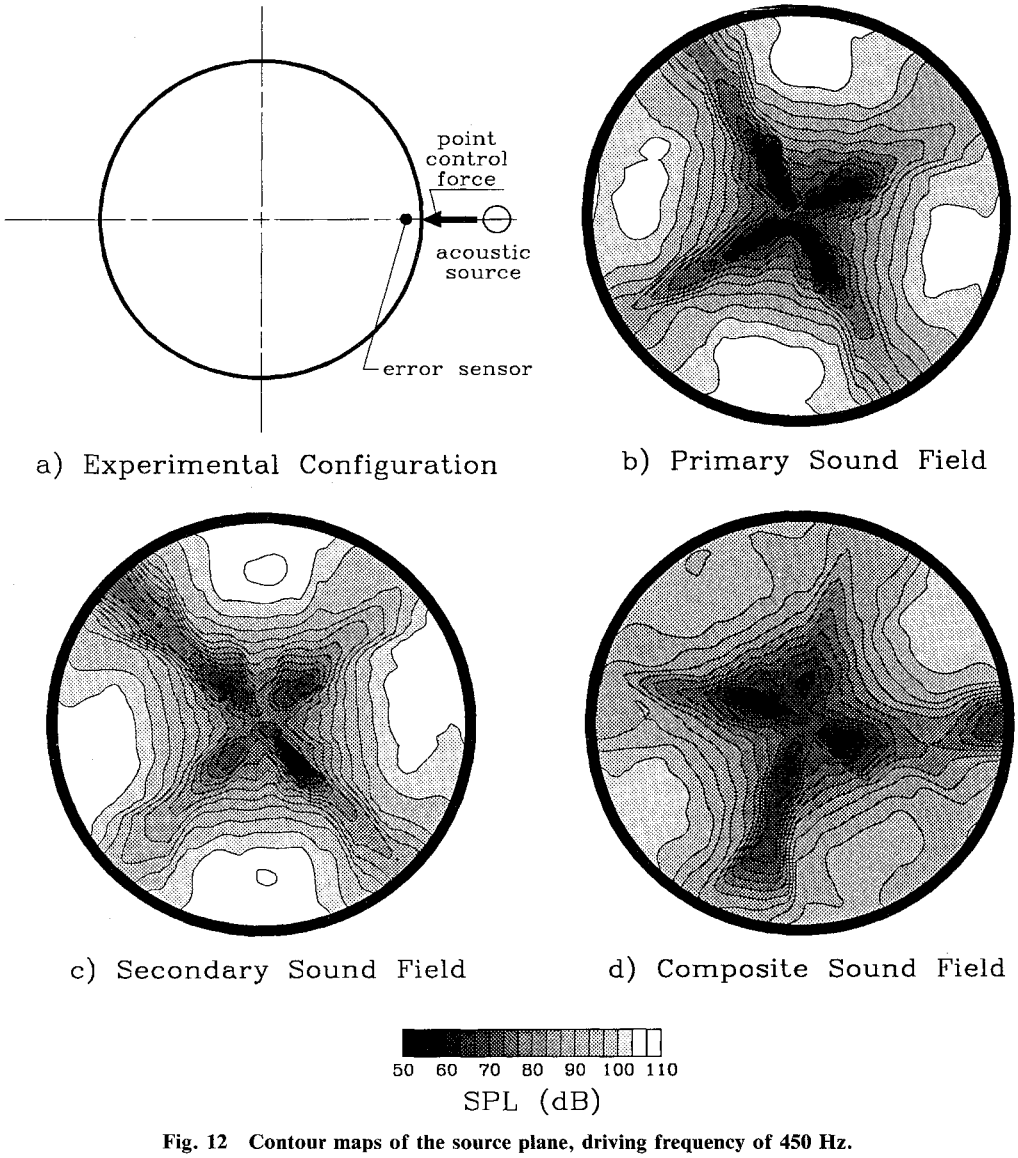


**Fig. 12 Contour maps of the source plane, driving frequency of 450 Hz.**

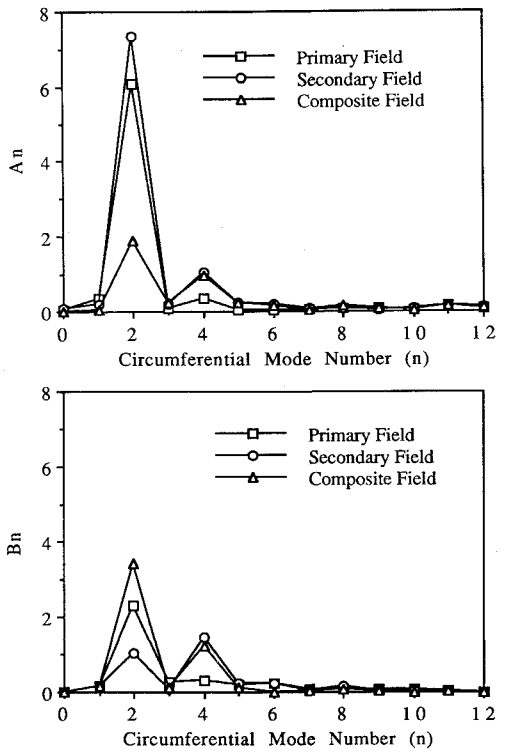


**Fig. 13 Relative modal amplitudes of pressure response in the source plane at 450 Hz: □, primary field; ○, secondary field; △, composite field.**

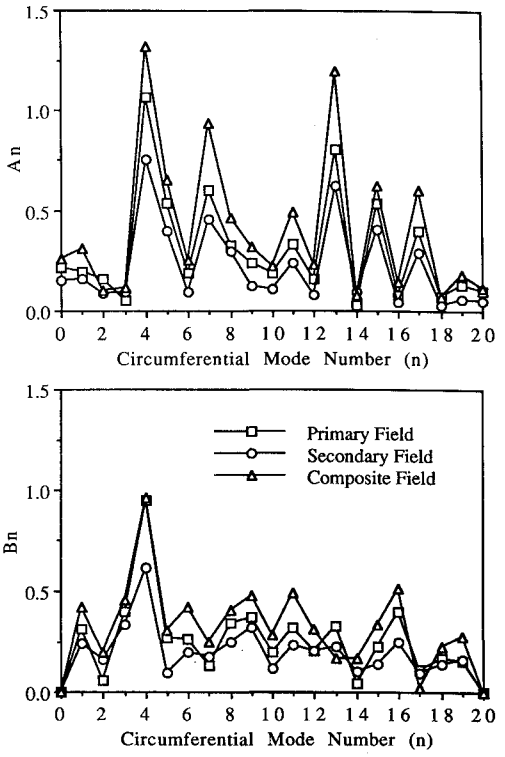


**Fig. 14 Relative modal amplitudes of the shell response in the source plane at 450 Hz: □, primary field; ○, secondary field; △, composite field.**

needed, as well as a control actuator that would couple well with it. Implementing a second error sensor and control source would likely improve the spatially averaged noise reduction.[7,8]

#### Test 2: 413 Hz

For this case, the system was driven at 413 Hz, a frequency at which the $n = 0$ mode dominates the interior acoustic field. During this test, the controller achieved 44.2 dB of control at the error location, with a corresponding spatially-averaged reduction of 27.6 dB.

The SPL contour plots for this case (Fig. 10) visually show that excellent global control was achieved at this frequency. This is possible because the $n = 0$ mode is not composed of two orthogonal components. When excited, the $a_0$ mode produces a constant level throughout the source plane (the $b_0$ mode is identically zero). Hence, only one error sensor is needed to fully describe the sound field, and one control source can spatially recreate it. A Fourier decomposition of the sound field for this case (Fig. 11) shows excellent control of the $a_0$ mode, with no corresponding increase in other acoustic modes of the cavity. This case represents the best possible results attainable with a one-channel controller for this type of system.

#### Test 3: 450 Hz

An excitation frequency of 450 Hz was chosen for this case. This is the lowest frequency for which the $n = 2$ mode dominates the interior sound field. The control algorithm achieved 52.6 dB of reduction at the error sensor for this case, although the spatially averaged reduction in the source plane was only 3.9 dB.

The SPL contour plots (Fig. 12) and Fourier decomposition (Fig. 13) show the dominance of the $n = 2$ mode at this frequency. The asymmetric $b_2$ mode was also excited by both the primary and secondary sources, as was the case in test 1 for the $n = 1$ mode, although the effect is not as severe in this case (the $a_2$ mode dominates). However, the separate $b_2$ components add to produce a higher composite $b_2$ magnitude in this case, whereas some level of reduction was achieved in the $b_1$ mode in test case 1. The extreme level of the $b_2$ mode in this case illustrates the need for at least two actuators and error sensors to provide better overall reduction. Implementing such a system would probably increase the spatially averaged noise reduction an additional 10–15 dB.[7,8]

Also evident in the Fourier decomposition for this case is a notable increase in the $n = 4$ acoustic mode ($a_4$ and $b_4$) caused by the control system. This was the first instance of energy spillover into higher-order acoustic modes for this series of tests. In order to better understand this phenomenon, acceleration of the shell was measured at 40 discrete locations in the source plane and a Fourier decomposition of the data was performed, with the results shown in Fig. 14. These data display a number of interesting features. Most evident are the dominant peaks at the $n = 4$, 7, and 13 structural modes. Results of an experimental modal analysis performed on this shell show three dominant peaks in this frequency range: one at 446 Hz, corresponding to an $n = 4$ mode shape; one at 440 Hz, corresponding to $n = 13$; and one at 465 Hz, corresponding to $n = 7$; so peaks at these values are expected. Note also that, for the $a_2$ structural mode, the level of excitation was reduced after the secondary field was applied. For most of the other modes, the level of excitation increased slightly, with increases generally being even over all of the modes. The overall acceleration level increased only 2.3 dB, indicating that control energy spillover into the shell is not a serious problem with this cylinder (at this frequency). This contrasts with previous studies,[7,8] which showed sharp increases in acceleration levels for select higher order modes but lower levels of excitation (from both sources) at lower order modes. The reduced level of control spillover in the current test shell is primarily due to the fact that the modal distribution of the primary and secondary sources are better matched. Although control spillover occurs in the shell, the spillover is predominantly constrained to the shell (except for the $n = 4$ mode) and thus does not corrupt the interior noise reduction. This behavior is a result of a selective modal filtering effect[6-8] (characteristic of the structural/acoustic interaction), which effectively filters the acoustic contributions of most of the uncontrolled structural modes in the shell. Finally, these results demonstrate that the

structural response of the shell at the $n = 4$ mode was sufficiently strong and well coupled with the interior acoustic space that energy spillover into the $n = 4$ acoustic mode occurred. To prevent this from happening, either a larger number of point controllers or a more distributed form of control force is needed.

**Test 4: 413 and 450 Hz**

In this case, the system was driven with two equal amplitude sinusoids at 413 and 450 Hz. As discussed previously, these two tones correspond to dominant $n = 0$ and $n = 2$ acoustic modes, respectively, within the cavity. This case was chosen to demonstrate that control of two independent modes at different frequencies is possible with a single control source and error sensor, as long as the control system is able to couple well with both modes. The controller achieved 53.9 and 53.5 dB of reduction of the 413 and 450 Hz tones, respectively, at the error sensor. The spatially averaged reduction in the source plane was 16.0 dB for the 413 Hz tone and the 10.3 dB for the 450 Hz tone. This compares with 27.6 and 3.9 dB of spatially averaged reduction at 413 and 450 Hz, respectively, when the tones were controlled individually. Hence, there is some compromise in the spatially averaged noise reduction at 413 Hz, but enhancement of the reduction at 450 Hz.

Contour plots of the overall sound level in the source plane are shown in Fig. 15. The spatially averaged noise reduction for the overall sound level in the source plane was 12.3 dB. From the composite sound field, it is obvious that the $b_2$ mode at 450 Hz was the limiting factor in terms of the spatially averaged noise reduction, as with case 3. Fourier decompositions of the individual interior pressure fields at 413 Hz and 450 Hz closely resemble those of Figs. 11 and 13, respectively.

**Test 5: Two Shakers at 450 Hz**

In this test, the effects of using an additional shaker, rather than an acoustic source, as the primary source were studied. This simulates a condition of localized vibrational energy flow into the shell, representative of structure-borne engine vibration traveling along an aircraft wing structure and exciting the fuselage at the spar attachment points. The control shaker was located at $\theta = 0$ deg, as before. The primary shaker was located at $\theta = 180$ deg (diametrically opposite the control source) and was driven at 450 Hz. Performance for this case was 57.7 dB of reduction at the error sensor and a spatially averaged reduction of 10.4 dB in the source plane.

Contour plots of the source plane are shown in Fig. 16, and Fourier decomposition of the sound field is shown in Fig. 17. Note that better global control is achieved for this case in comparison with test 3 because the control source is more closely matched with the primary source in terms of modal distribution. Since both the primary and secondary actuators are pointwise force inputs, the interior fields created by each will be spatially similar and will provide better global control. This result suggests that localized energy flow into a structure (e.g.,

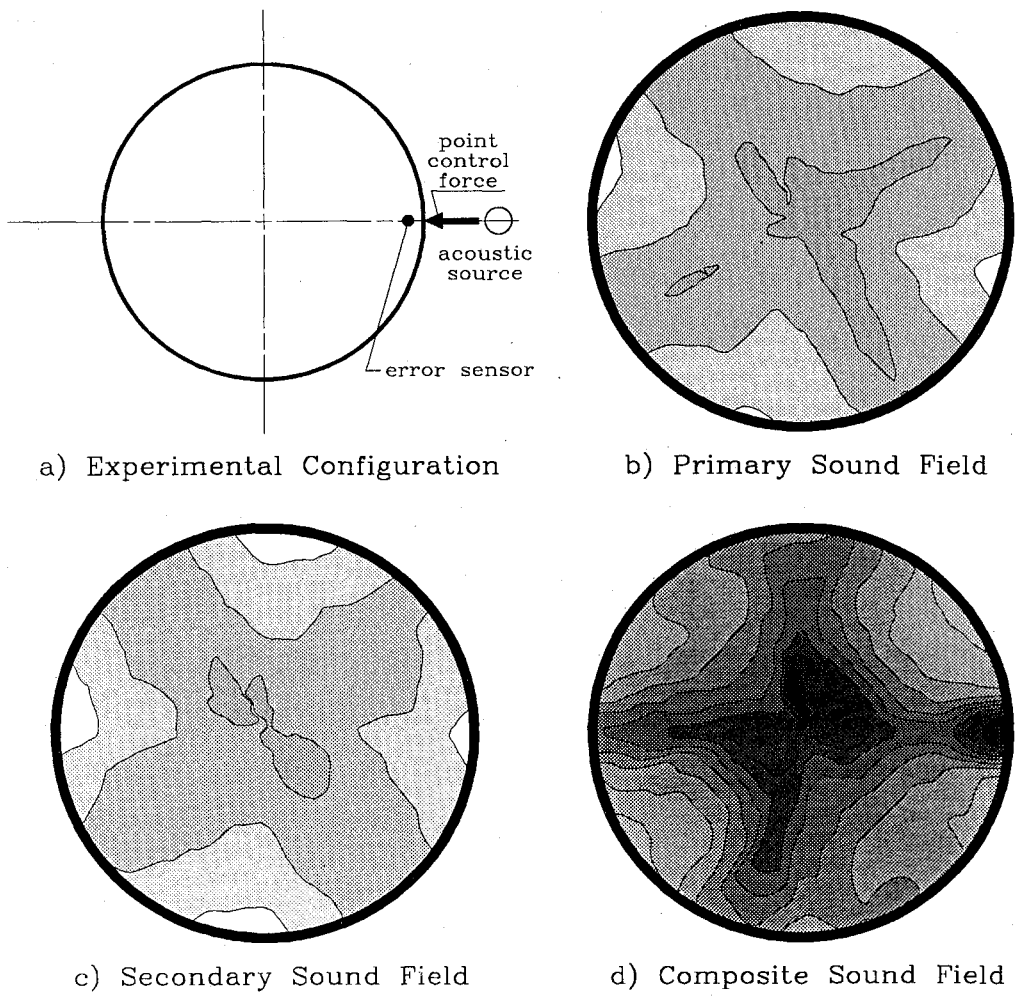


**Fig. 15 Contour maps of the source plane, driving frequency of 413 and 450 Hz.**

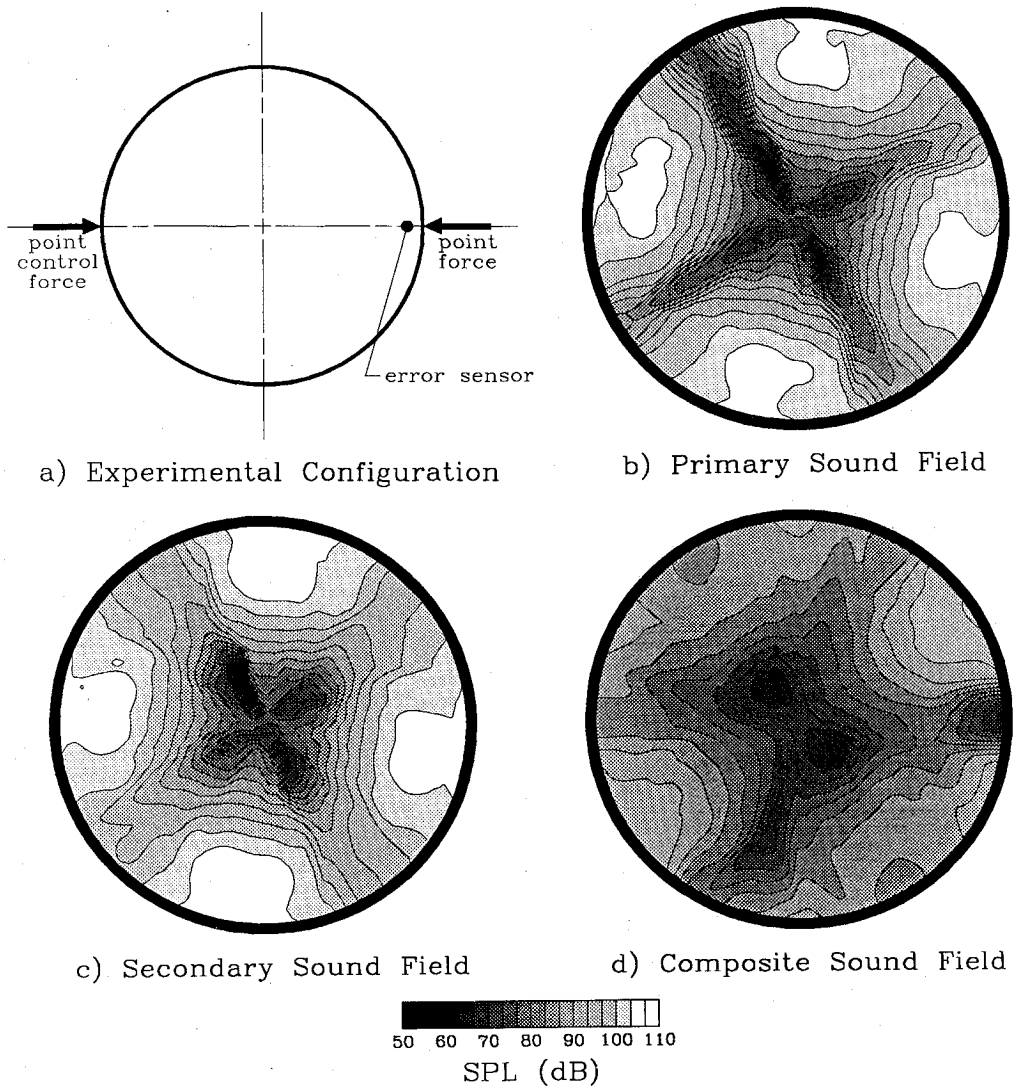


**Fig. 16 Contour maps of the source plane, driving frequency of 450 Hz.**

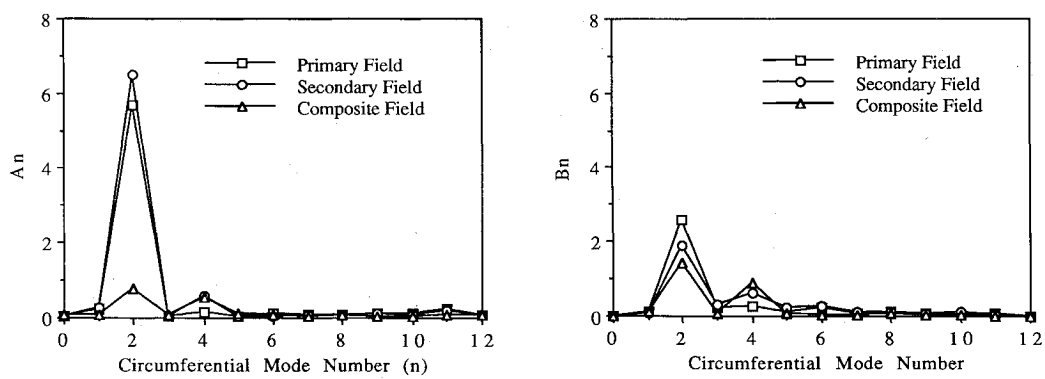


**Fig. 17 Relative modal amplitudes of pressure response in the source plane at 450 Hz: □, primary field; ○, secondary field; △, composite field.**

at an engine pylon or wing spar attachment) may be easier to control with point vibration controllers than distributed energy flow (e.g., airborne propeller-induced cabin noise).

## Conclusions

A simplified model of an aircraft fuselage was used to evaluate an ANC system. The primary test configuration consisted of external horn drivers as the primary source and a mini-shaker attached pointwise to the shell wall as the secondary controller. A second test configuration used a mini-shaker in place of the horn drivers as the primary source. A single input/single output control system based on the filtered-$x$ version of the LMS algorithm was developed to optimize the signal to the control shaker. The results of this investigation revealed several important conclusions.

1) The alignment of the acoustic mode shapes within the shell are affected by inhomogeneities in the shell and the mini-shaker attachment to the shell.

2) Control spillover in the shell vibration is minimal when the primary and secondary sources are reasonably well-matched in modal distribution.

3) In general, control of multiple modes at the same frequency will require an equal number of controllers to optimize the performance of the control system.

4) Two or more modes at different frequencies can be controlled with a single controller if the control system can detect and couple with each mode of interest.

5) Localized energy flow into a structure may be easier to control than distributed energy flow when point vibration controllers are used.

## Acknowledgments

The authors gratefully acknowledge the support of this work by the National Science Foundation under grant MSM-8810384, and the Motorola Corporation for their donation of the Motorola DSP56000 Application Development System, which was used in this research.

## References

[1]May, D. N., and Meade, J. P., "Exterior Noise of the McDonnell Douglas UHB Demonstrator," *Proceedings of Inter-Noise 89,* Noise Control Foundation, New York, 1989, pp.227–232.

[2]Zalas, J. M., and Tichy, J., "Active Attenuation of Propeller Blade Passage Noise," NASA CR 172386, July 1984.

[3]Lester, H. C., and Fuller, C. R., "Active Control of Propeller Induced Noise Fields Inside a Flexible Cylinder," AIAA Paper 86-1957, July 1986.

[4]Silcox, R. J., Lester, H. C., and Abler, S. B., "An Evaluation of Noise Control in a Cylindrical Shell," NASA TM-89090, Jan. 1987.

[5]Bullmore, A. J., Nelson, P. A., Elliott, S. J., Evers, J. F., and Chidley, B., "Models for Evaluating the Performance of Propeller Aircraft Active Noise Control Systems," AIAA Paper 87-2704, Oct. 1987.

[6]Jones, J. D., and Fuller, C. R., "Reduction of Interior Sound Fields in Flexible Cylinders by Active Vibration Control," *International Journal of Analytical and Experimental Modal Analysis,* Vol. 4, No. 2, 1989, pp. 45–50.

[7]Jones, J. D., and Fuller, C. R., "Active Control of Structurally-Coupled Sound Fields in Elastic Cylinders by Vibrational Force Inputs," *International Journal of Analytical and Experimental Modal Analysis,* Vol. 5, No. 3, 1990, pp. 123–140.

[8]Jones, J. D., and Fuller, C. R., "Active Control of Sound Fields in Elastic Cylinders by Multi-Control Forces," *AIAA Journal,* Vol. 27, No. 7, 1989, pp. 845–852.

[9]Simpson, M. A., Luong, T. M., Fuller, C. R., and Jones, J. D., "Full-scale Demonstration Tests of Cabin Noise Reduction Using Active Vibration Control," AIAA Paper 89-1074, April 1989.

[10]Elliott, S. J., Nelson, P. A., Stothers, I., Boucher, C., Evers, J., and Chidley, B., "In-Flight Experiments on the Active Control of Propeller- Induced Cabin Noise," AIAA Paper 89-1047, April 1989.

[11]Widrow, B., and Stearns, S. D., *Adaptive Signal Processing,* Prentice Hall, Englewood Cliffs, NJ, 1985, Chap. 6.

[12]Jones, J. D., and Fuller, C. R., "An Experimental Investigation of the Interior Noise Control Effects of Propeller Synchrophasing," NASA CR-178185, Oct. 1986.